Journal of Sustainable Metallurgy (2023) 9:522–536
https://doi.org/10.1007/s40831-023-00665-6

RESEARCH ARTICLE

Mechanical Activation-Assisted Recovery of Valuable Metals from Black Mass in the Form of Fe/Cu Alloys

Safoura Babanejad[1] · Hesham Ahmed[1,2] · Charlotte Andersson[1] · Eetu-Pekka Heikkinen[3]

Received: 16 July 2022 / Accepted: 17 February 2023 / Published online: 6 March 2023

Abstract

Pyrometallurgy is a popular industrial method that is employed in the recovery of valuable elements from black mass (BM), which is produced by pretreatment of Li-ion batteries. This method struggles with some downsides, such as the incineration of graphite and high energy consumption. In this study, the goal is to utilize graphite in the BM to produce a master alloy in an attempt to decrease the energy input requirement. To achieve this, metal oxides (Fe_2O_3 and CuO) are added to the BM to produce an Fe/Cu-based alloy containing Co/Ni as alloying elements. Mechanical activation is also employed to decrease the energy requirement and to increase the amount of metal oxide that can be reduced by the graphite in the BM. The results revealed that it is possible to produce the aforementioned alloys, the efficiency of which can be improved by applying mechanical activation. After 1 h of milling, the required heat flow for producing Fe- and Cu-based alloys is lowered for ~10 and ~25 kWh, respectively. Plus, the direct CO_2 emission decreases for 13–17% in the iron system and 43–46% in the copper system.

Graphical Abstract

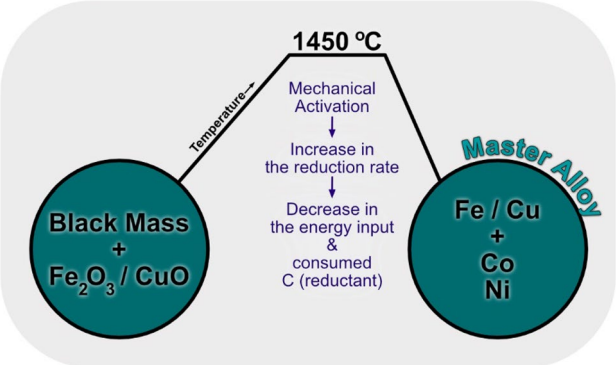

Keywords Li-ion batteries · Black mass · Pyrometallurgy · Alloy · Mechanical activation · Mass and energy balance

The contributing editor for this article was Markus Reuter.

✉ Safoura Babanejad
safbab@ltu.se

✉ Hesham Ahmed
hesham.ahmed@ltu.se

[1] Department of Civil, Environmental and Natural Resource Engineering, Process Metallurgy, Minerals and Metallurgical Engineering, Luleå University of Technology, 971 87 Luleå, Sweden

[2] Central Metallurgical Research and Development Institute, P.O. Box 87, Helwan 114 21, Egypt

[3] University of Oulu, Process Metallurgy, PO Box 4300, 90014 Oulu, Finland

Abbreviations

LIB	Li-ion battery
EU	European Union
BM	Black mass
MeO	Metal oxide
$LiMeO_2$	Li metal oxide
LCO	A type of battery consisting of $LiCoO_2$ as the cathode material and graphite as the anode material
NMC	A type of battery consisting of $LiNi_xMn_yCo_zO_2$ (in this study: $x=y=z=0.33$) as the cathode material and graphite as the anode material
TGA	Thermogravimetric analysis
PSD	Particle size distribution
XRD	X-ray diffraction

Introduction

"Lithium-ion batteries have indeed become the critical pillar for building a fossil fuel-free economy" [1]. The consumption of fossil fuels has led to global warming. This issue drag the public attention to renewable energies, which are not applicable unless by using rechargeable batteries, especially LIBs [2]. The production technologies for manufacturing batteries have been developed significantly in the recent years; New battery chemistries have been introduced, new manufacturing methods have been developed, and scale of manufacturing has increased. These have led to a price drop (almost 90% since 2010) in the LIBs for electric vehicles [3]. This drop in the manufacturing costs make the recycling seem costly. Moreover, the global recycling rate of LIBs is already low today, with less than 5% of LIBs being recycled in 2020 [1]. Hence, if efficient and economical recycling methods are developed, the recovery of LIB elements would replace the extraction of these elements from primary resources. It will have a direct effect on the economic and resource issues in this sector. The importance of recycling and its positive outcome has also been asserted by the EU Battery Directive (2006/66/EC) [4]. Co, graphite, and Li (key elements in a broad range of portable batteries and electric vehicles) are known as critical raw materials in the EU due to limitations in their geological availability, geopolitics, and market [5, 6].

The recycling methods mostly begin with a pretreatment step that can be mechanical, chemical, or thermal. During pretreatment step, the LIB particles are liberated and the critical and precious elements are concentrated in a fine fraction, called black mass (BM) [7, 8]. The main process to recover valuable metals from BM is either hydrometallurgical, pyrometallurgical, or a combination of these two. In stand-alone hydrometallurgical processes, such as Recupyl and Batrec, special attention is given to pretreatment to prepare the BM for subsequent leaching and solvent extraction. While in the pyrometallurgical process, e.g., Inmetco and Glencore, an alloy consisting of Ni, Co, Cu and Fe is produced with Al and Li accumulated in a slag phase. Thereafter, the produced alloy can be refined in a hydrometallurgical procedure, as is done in Umicore [9–11].

Compared to hydrometallurgical, the advantages of the pyrometallurgical methods can be listed as follows: (i) it is more flexible since the technology does not need to be specified for different LIB types and some of the current technologies are capable of recycling all types of batteries, e.g., Valdi, Glencore, and Dowa; (ii) there are high capacity available technologies; and (iii) the passivation step is not necessarily required [7, 12]. However, high energy demand plus CO_2 emission limits the implementation of pyrometallurgical processes [12, 13]. Since the pyrometallurgical process is done at elevated temperatures, in an oxidative atmosphere, graphite can burns out, like what occurs during incineration [14–16]. If the process would be in a reductive atmosphere, graphite can be used as a reducing agent, although the graphite in the BM is more than the required C for the reduction of $LiMeO_2$ in the BM. It can thus be expected that part of the graphite remains unreacted after reduction [17–20].

A decrease in working temperature of a pyrometallurgy process would lower the energy consumption in this method. To achieve this, mechanical activation can be employed. Mechanical activation of minerals and mixed oxides through milling decreases the particle size and increases their energy state, which leads to an increase in the thermal reactivity and subsequently a decrease in the required working temperature. Mechanical activation of, for example, hematite concentrate, galena, and pyrite has been investigated, and their thermal behaviour was compared to that of nonactivated minerals. The reduction temperature of hematite as well as thermal decomposition of galena and pyrite was lowered significantly [21–26]. It has been reported that the mechanical activation of carbon-containing mixed oxide systems enhances the carbothermic reduction kinetics [27]. BM is also a material containing C and MeOs, however, the effect of mechanical activation on its thermal behaviour has not been studied thus far.

In the known pyrometallurgical recovery methods, the graphite in the BM is mostly incinerated before or during melting, which is not a proper method for its utilization. On the other hand, the process is energy-intensive, where mechanical activation can be a method for lowering energy consumption during recovery. In the current study, a pyrometallurgy-based method is proposed for recycling of LIB components. This study aims at taking advantage of the graphite present in the BM. Two different MeOs (Fe_2O_3 and CuO) were added to the BM to utilize its graphite as a reducing agent. The feasibility of producing a master alloy

containing Co/Ni (in the BM) as alloying elements was assessed. Additionally, mechanical activation was employed as a process for creating disorder and defects in the lattice structure and increasing the active surface area to increase the reduction efficiency of the BM or BM/MeO mixture by changing the required energy and C consumption.

Experimental

Materials

The BMs from LCO and NMC LIBs were provided by Stena Recycling International AB, Sweden. Samples with a particle size of 150–700 µm were the focus of the present investigation, and their detailed description was given in an earlier publication [28]. Their composition is listed in Table 1. Fe_2O_3 (−325 mesh, 98%, Alfa Aesar) and CuO (97.5%, AnalaR NORMAPUR) were utilized in the alloying trials.

Characterization

A PSD analyzer (Retsch Camsizer XT) was utilized in this study to determine the size of the BM particles. A PANalytical Empyrean X-ray diffractometer using CuKα radiation (λ = 0.154184 nm) was used in a 2θ range of 10–90° with a step size of 0.026°/s. Phase identification was performed using HighScore Plus software (v4.7, PANalytical B.V., Almelo, The Netherlands). To analyze the C content in the BM, an EA3000 CHNS-O elemental analyzer from Eurovector Srl was employed (DIN 51,732). Inductively Coupled Plasma–Mass Spectrometry (ICP–MS) was used to analyze the chemical composition. The analysis was done according to SS EN ISO 17294–2:2016 and EPA method 200.8:1994.

Reduction-Alloying Trials

Initially, Fe/Cu oxides were added to the BM to utilize its excess graphite and to produce Fe/Cu-based alloys. The MeOs were mixed with BM in such a way that the net C/O molar ratio was equal to unity. The C content of the BM was accounted for in this C/O molar ratio. O in the cathode active material plus O in the added MeO (Fe_2O_3 or CuO) were considered as the reducible O in the C/O molar ratio. In this regard, the ratio of added MeOs to the BM is listed in Table 2. In the following parts of this paper, the prepared mixtures will be addressed as noted in this table.

Table 2 Description of utilized mixtures

Mixture	MeO (g):BM (g)
MixFeLCO	55.0:45.0 Fe_2O_3:LCO
MixFeNMC	60.5:39.5 Fe_2O_3:NMC
MixCuLCO	59.5:40.5 CuO:LCO
MixCuNMC	67.0:33.0 CuO:NMC

Second, a Fritsch Pulverisette 7 Planetary micromill was used to mechanically activate the BM and MeO-BM mixtures. The 80 ml cups in this ball mill consisted of 10 hardened steel balls with a diameter of 15 mm. To avoid excessive heat during milling, each 30 min of milling was followed by 15 min of cooling. The sample-to-balls ratio and rotating speed were fixed to 20 g of sample and 10 balls and 700 rpm, respectively, for the predetermined periods.

The prepared BM and MeO-BM mixtures underwent reduction-alloying experiments utilizing TGA (Netzsch STA 409) with a detection limit of 1 µg and an Ar flow rate of 100 ml/min. ~1 g sample was used in each experiment. In the trials applied on the BM, the temperature was increased linearly at a heating rate of 10 °C/min up to 1100 °C. The heating was followed by linear cooling to 200 °C at a rate of 20 °C/min. In the MeO-BM mixture trials, the samples were heated linearly up to 1450 °C at a heating rate of 10 °C/min, held at that temperature for 1 h, and then cooled to 200 °C at a rate of 20 °C/min.

Thermodynamic Modeling

FactSage 8.0™ software has been utilized as a thermodynamic calculation tool to study the reactions occurring at high temperature [29]. The Equilib module, employing FactPS, FToxid, and FTmisc databases, was used in these calculations. The ideal gas and pure solids as the main species along with the solution phases, as listed below, were considered:

- *FToxid-SLAGA*;
- *FToxid-SPINA*;
- *FToxid-MeO_A;*
- *FToxid-NAShB*;
- *FToxid-NASlB*;
- *FTmisc-FeLQ*; and
- *FTmisc-CuLQ* (since Co is not included in this solution phase, *Co(liq)* was added as an ideal solution).

Table 1 The chemical compositions of LCO and NMC BM (wt. %) [28]

Sample (wt.%)	Li	Co	Ni	Mn	Al	Cu	Si	P	F	C
LCO BM	4.0	32.3	0.0	0.0	0.9	0.6	1.6	0.5	2.6	35.4
NMC BM	3.6	8.0	7.3	7.6	0.2	1.6	1.0	0.6	6.5	43.2

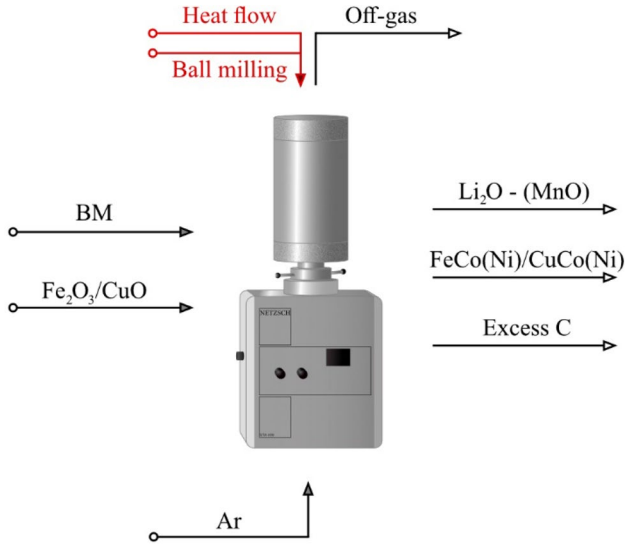

Fig. 1 Input and output flows used in the mass and energy balance

Mass and energy balances were made to estimate the energy requirements, the exergy loss, as well as CO_2 emissions of different cases and they were made by means of HSC Chemistry v. 10.0.7 and the regarded databases. The key elements during reduction were considered in these calculations, i.e., Co, Ni, Mn, C, Fe, O, and Li. The input and output flows were designed as demonstrated in Fig. 1. The output components were selected based on the results from XRD and FactSage modeling, which will be discussed later in this manuscript.

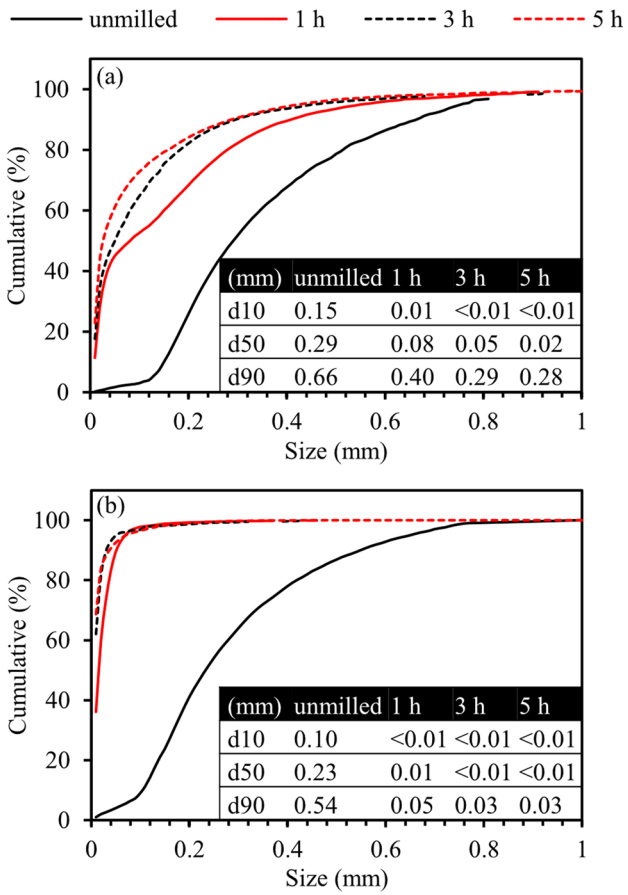

Fig. 2 Cumulative PSD of **a** LCO BM and **b** NMC BM under four conditions: unmilled, milled for 1 h, milled for 3 h, and milled for 5 h

Results and Discussion

Effect of Mechanical Activation on BM Reduction

The PSD of the BM before and after milling from the LCO and NMC is given in Fig. 2. The d10, d50, and d90 values are also listed in Fig. 2. d10 decreases by 10 times in both BM types after 1 h of milling, and a further decrease is not distinguishable with the utilized equipment. The average particle size (d50) for the LCO BM is 0.29 mm in the unmilled sample, which decreases drastically to 0.08, 0.05, and 0.02 mm after 1, 3, and 5 h of milling, respectively. The lowest effect is on the d90 value, which decreases by 40% after 1 h of milling and ~60% after 3 and 5 h. In the NMC BM, d50 and d90 decrease by 96 and 90%, respectively, after 1 h of milling, while longer milling periods do not influence the particle size considerably.

The effect of milling on thermal reactivity was further studied using TGA. Figure 3 shows the mass loss as a function of temperature at different milling times. Mass loss begins at ~200–300 °C and continues until ~600 °C in both types of BM. The curves of the mixtures with different milling times overlap in this period, while after ~600 °C, they do not follow the same rate, and at a fixed temperature, different mass losses are observed in these samples. As an example, in the LCO BM at 800 °C, a mass loss of 16% occurs in the unmilled samples, which increases to 23% in the samples milled for 1 and 3 h. The mass loss decreases to 19% after milling for 5 h. The change in the NMC BM mass loss, caused by mechanical activation, can be better observed at ~650 °C, where the mass loss is 10% in the unmilled sample and 13, 13, and 17% in the samples milled for 1, 3, and 5 h, respectively. Generally, it can be stated that after 1 h of milling, an increase in the mass loss rate is observed, while 3 h of milling does not cause any changes to the BM compared with the BM milled for 1 h. After 5 h of milling, the mass loss rate in the LCO BM decreases, and in the NMC BM, it increases slightly.

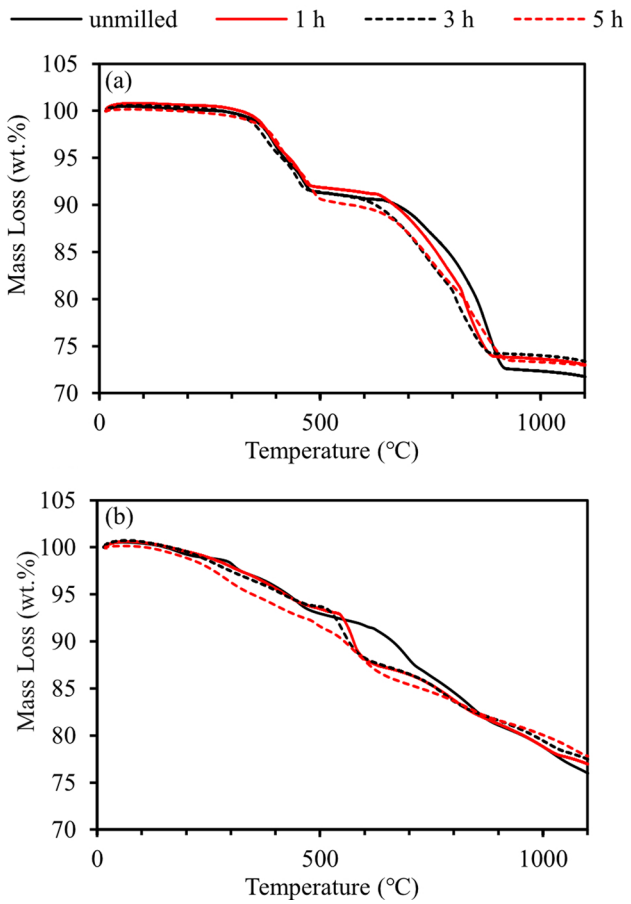

Fig. 3 Mass loss as a function of temperature during the reduction of **a** LCO BM and **b** NMC BM before and after milling for 1, 3, and 5 h

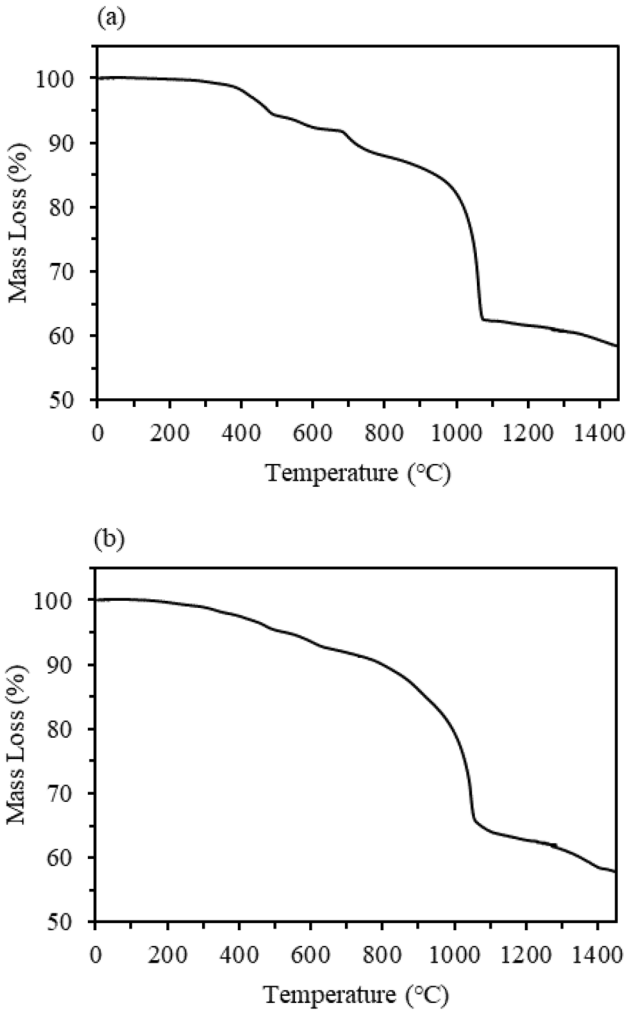

Fig. 4 Mass loss as a function of temperature during the reduction of **a** MixFeLCO and **b** MixFeNMC

The TGA graphs reveal that the main effect of mechanical activation on the reaction kinetics of BM is after 600 °C, which is the temperature at which the cathode material ($LiCoO_2$ in LCO BM and $LiNi_{0.33}Mn_{0.33}Co_{0.33}O_2$ in NMC BM) transforms to simpler oxides [28]. Since the reactions were triggered when the temperature was not constant and it was gradually increasing, the reduction reaction shifted to a lower temperature range. In other words, the increase in the reduction rate, after 600 °C, lowers the temperature of the subsequent reduction of produced oxides (Co and Ni oxides).

Generally, the reduction behaviour of BM with different periods of mechanical activation shows that milling affects the reduction temperature of BM after transformation of the cathode material to its constituent oxides. Regarding the milling periods, it was seen that milling for 1 and 3 h has almost the same effect and shift the reduction to a lower temperature range. Milling for 5 h had an opposite effect in the LCO BM and a negligible effect in the NMC BM.

Reduction Behaviour of MeO-BM Mixture

To maximize the utilization of graphite and produce Fe/Cu-based alloys, Fe_2O_3 and CuO were added as described in Table 2.

Iron System

The mass loss during heating of the Fe_2O_3-BM mixture is plotted in Fig. 4. Mass losses of 44 and 43% for MixFeLCO and MixFeNMC are recorded until 1450 °C, respectively. The mass loss begins at 150–200 °C and continues until 1450 °C for both BMs.

The reduction of Fe_2O_3 occurs in multiple steps by reduction to Fe_3O_4, FeO, and finally Fe, which has been explained thoroughly in the literature [30, 31]. All these occurring

reduction reactions result in different slopes in the mass loss trend; since this is not the concern of this study, the details will not be investigated in this article. According to the literature, the reduction of Fe_2O_3 to Fe is complete after reaching a temperature of ~ 1150 °C [30]. The continuation of mass loss at temperatures higher than 1200 °C (with a different mass loss rate) can be attributed to the late reduction of some oxides. This can also be due to the reaction of irreducible oxides (by carbon under the present experimental conditions) such as Li_2O and MnO with F, which produces Li/Mn fluorides and O. O can then react with graphite and produce CO.

FactSage predicts the phases that are thermodynamically stable at 1450 °C. The results are presented in Fig. 5. All Fe_2O_3 is reduced to Fe alloys together with Co (and Ni in MixFeNMC) in the BM. Almost all Li remains in the slag phase (in the form of oxide and fluoride), Mn remains mainly in the oxide form, and the rest forms fluoride. Furthermore, no graphite remains after reduction, which is mainly related to the fact that thermodynamically CO is the only gaseous product of reduction of metal oxides at 1450 °C [28]. However, during the experiment, the reduction begins at lower temperatures where both CO and CO_2 are produced. Compared to CO as a reduction product, CO_2 production consumes less C. Hence, the C analysis indicates that graphite remains in the sample after reduction, which is not in line with the FactSage calculations at 1450 °C.

Copper System

Figure 6 presents the mass loss of the CuO-BM mixture as a function of temperature during heating in a reductive atmosphere. 33 and 30% mass losses occur in MixCuLCO and MixCuNMC, respectively. The mass loss starts at ~250 °C and continues until 1450 °C.

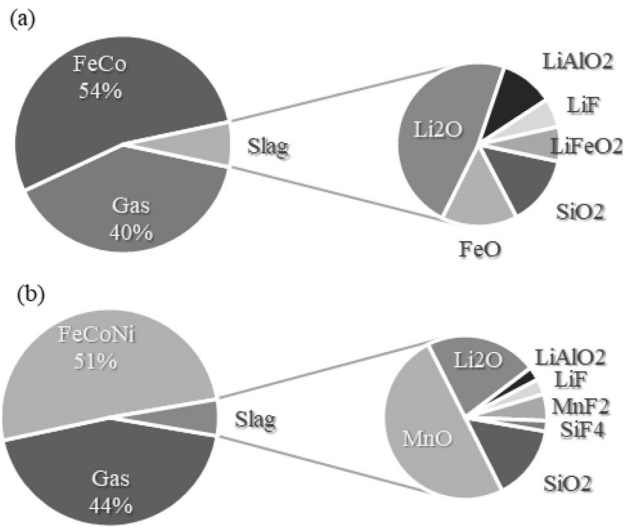

Fig. 5 **a** MixFeLCO and **b** MixFeNMC reduced at 1450 °C, calculated by FactSage: Phase distribution and slag calculated components

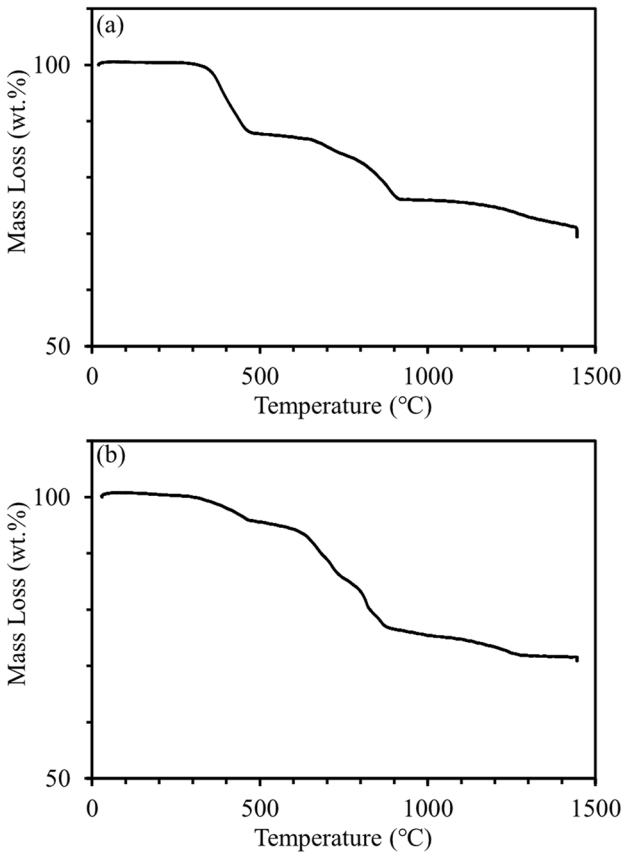

Fig. 6 Mass loss as a function of temperature during the reduction of **a** MixCuLCO and **b** MixCuNMC

Based on FactSage calculations, in the presence of CuO and C, Cu is thermodynamically stable at room temperature. It has been reported that practically, reduction begins at higher temperatures; for instance, 440 °C was reported in a study as the starting point of CuO carbothermic reduction [32]. In general, the reduction starting temperature depends on kinetic factors, such as the heating rate, the particle size, and the contact between the reducing agent and CuO. In the current study, CuO reduction begins at ~300 °C. The change in the mass loss at ~600 °C can be related to the transformation of $LiCoO_2$/$LiNi_{0.33}Mn_{0.33}Co_{0.33}O_2$ that has been discussed previously. Thermodynamic modeling reveals that Cu begins to melt at ~1000 and ~800 °C in MixCuLCO and MixCuNMC, respectively. The continuation of the mass loss at higher temperatures, as explained in the iron system, can be due to (i) the late reduction of the remaining oxides or (ii) the reaction of the irreducible oxides with F.

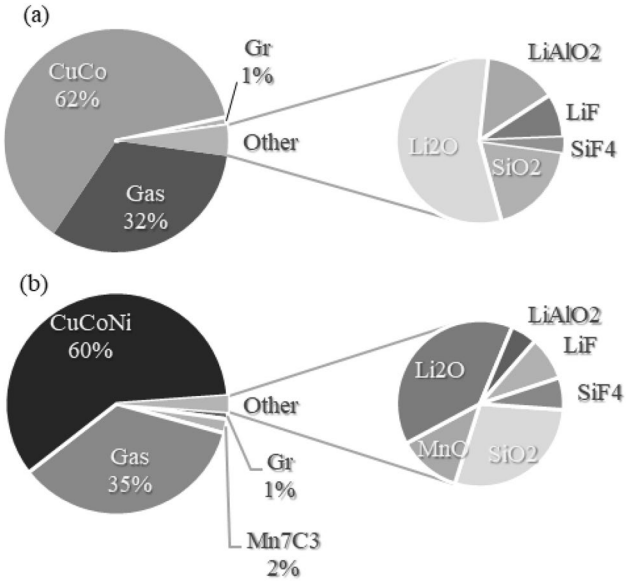

Fig. 7 **a** MixCuLCO and **b** MixCuNMC reduced at 1450 °C, calculated by FactSage: Phase distribution and slag calculated components

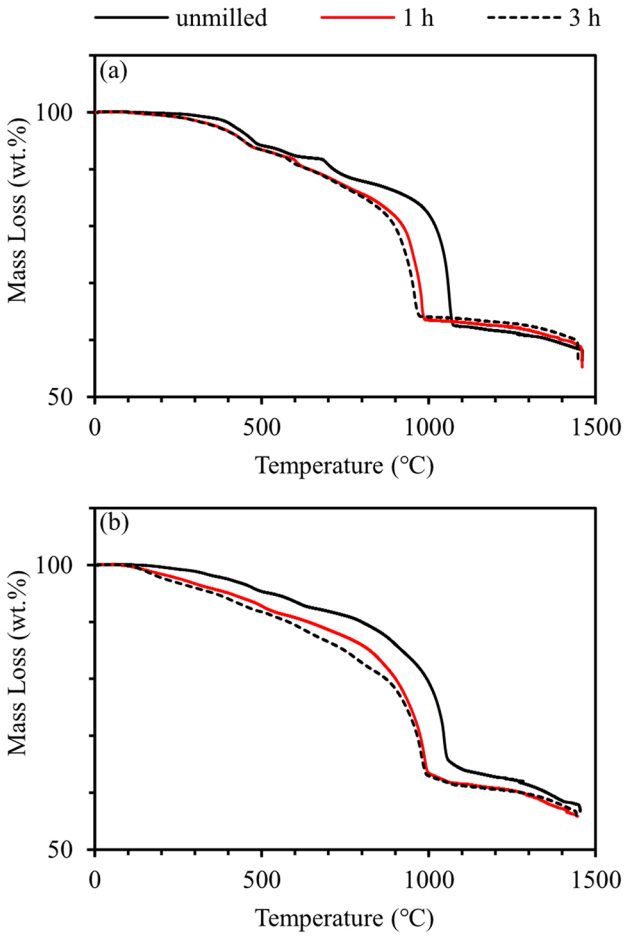

Fig. 8 Mass loss as a function of temperature during the reduction of **a** MixFeLCO and **b** MixFeNMC before and after milling for 1 and 3 h

According to the results obtained from FactSage calculations at 1450 °C (Fig. 7), Cu-based alloys are the main products of the reduction. It seems that part of the excess graphite in MixCuNMC forms Mn carbide. Generally, in both systems, the slag compositions demonstrate that Li_2O, $LiAlO_2$, and LiF are thermodynamically the Li-containing compounds at that temperature.

Effect of Mechanical Activation on the Reduction of MeO-BM Mixture

TGA of the BM in Sect. "Effect of Mechanical Activation on BM Reduction" showed that milling for 5 h in the LCO BM is not beneficial, and in the NMC BM, is very insignificant, which makes further milling (5 h) unnecessary from an energy point of view. On the other hand, it has been observed that milling for 1 and 3 h has the same effect on the reduction of BM. Accordingly, 5 h of milling was omitted for the mixture of Fe_2O_3 and BM, while the condition of 3 h of milling was kept examining whether it has any significant influence with the addition of MeO.

Iron System

Figure 8 illustrates the mass loss profile of Fe_2O_3-BM mixtures with different periods of milling. The curves show the different behaviours in general. To observe this more specifically, the mass loss of the Fe_2O_3-LCO mixture at 900 °C is taken into account. A mass loss of 12% is recorded at that temperature for the unmilled sample, which increases to 18% after milling for 1 h, and the mass loss difference between the mixture milled for 1 h and the one milled for 3 h is only 2%. Considering the same temperature in the Fe_2O_3-NMC mixture, the mass loss increases from 14% in the unmilled mixture to 20 and 22% in the mixtures milled for 1 h and 3 h, respectively. Generally, a significant effect is observed after 1 h of milling, while the effect of milling for 3 h compared to 1 h is negligible.

XRD measurements were performed on several samples with the same composition but different mechanical activation periods. For simplicity, only one measurement for each composition is presented. The reduced samples of mixtures milled for 1 h were selected for XRD measurements. Figure 9 demonstrates the XRD patterns of the

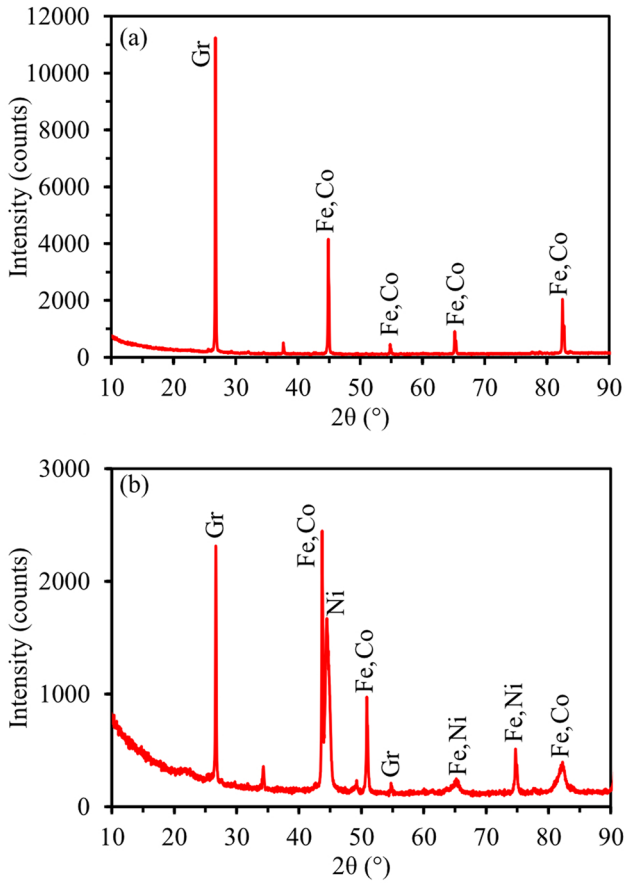

Fig. 9 XRD patterns of reduced **a** MixFeLCO and **b** MixFeNMC milled for 1 h

reduced Fe_2O_3-BM mixtures milled for 1 h. Peaks attributed to graphite (represented as Gr in the graphs) and metallics such as Fe, Co, and Ni are detected in these patterns. The interaction of the Fe matrix with Cu-tube radiation should also be taken into consideration. This interaction leads to fluorescence that increases the background level; hence, it is not reliable to compare the peak intensities in the pattern [33].

The chemical composition of unmilled and milled mixtures after reduction is listed in Table 3. The main elements in the BM plus Fe in the added MeO are considered as the main elements, and the rest are reported as *other*. The main effect can be observed for the amount of C remaining in the reduced mixture, which increases with increasing milling time. The remaining C is almost constant after 1 and 3 h of milling.

The results in Fig. 8 show that mechanical activation affects the reduction rate after ~600 °C, and this effect continues to the temperature of ~1100 °C. Jung and Yi [30] stated that the reduction of FeO to Fe is completed at 1147 °C, the temperature at which the milling effect ends based on Fig. 8 [30].

The XRD patterns in Fig. 9 show that Fe-based alloy and graphite are both present in the sample. The chemical analysis of unmilled reduced mixtures (Table 3) also shows that C remains after reduction. It can be perceived that although Fe_2O_3 was added based on the C:O molar ratio of one, the graphite in the BM is capable of reducing more oxide. By increasing the milling time (especially after 1 h) and consequently decreasing the temperature range in which the reduction takes place, the amount of excess C (remained after reduction) increases. To explain this matter, the Boudouard reaction should be taken into account, which discusses the partial pressure of CO/CO_2 by changing the temperature in Eq. 1. Based on this reaction, by decreasing the temperature, the partial pressure of CO_2 increases. The production of CO_2 in a reduction reaction consumes less C compared to a reaction with CO as a product.

$$C + CO_2 \rightleftharpoons 2CO \tag{1}$$

To investigate this further, mass and energy calculations were performed to study the effect of a longer milling time on the required heat input for the system. Furthermore, the CO and CO_2 contents in the off-gas were calculated using the final excess carbon as a variable. The calculation results are shown in Fig. 10. The modeling indicates that by increasing the milling time, there is a decrease in the required input heat flow, which is accompanied by a decrease in CO and an increase in CO_2 content in the off-gas. This is what was expected from the TGA results (Fig. 4), i.e., by increasing the reduction rate, the reduction takes place in a lower

Table 3 Chemical composition of unmilled and milled Fe_2O_3-BM mixtures after reduction at 1450 °C

Mixture	Milling time	Chemical composition						
		Fe	Co	Mn	Ni	C	Li	Other
MixFeLCO	Unmilled	63.4 ± 0.2	26.9 ± 0.0	0.0	0.0	3.2 ± 0.0	2.3 ± 0.5	4.2
	1 h	62.7 ± 0.3	26.3 ± 0.0	0.0	0.0	6.0 ± 0.2	1.5 ± 0.3	3.4
	3 h	61.1 ± 1.0	26.1 ± 0.4	0.0	0.0	6.8 ± 0.1	2.5 ± 0.5	3.5
MixFeNMC	Unmilled	68.9 ± 0.0	8.2 ± 0.0	6.5 ± 0.0	7.5 ± 0.0	3.5 ± 0.0	2.5 ± 0.5	2.9
	1 h	70.5 ± 0.5	6.2 ± 0.1	5.2 ± 0.0	6.0 ± 0.1	7.6 ± 0.4	2.3 ± 0.5	2.3
	3 h	69.5 ± 0.9	6.4 ± 0.1	5.4 ± 0.1	6.1 ± 0.1	7.7 ± 0.3	2.9 ± 0.6	2.0

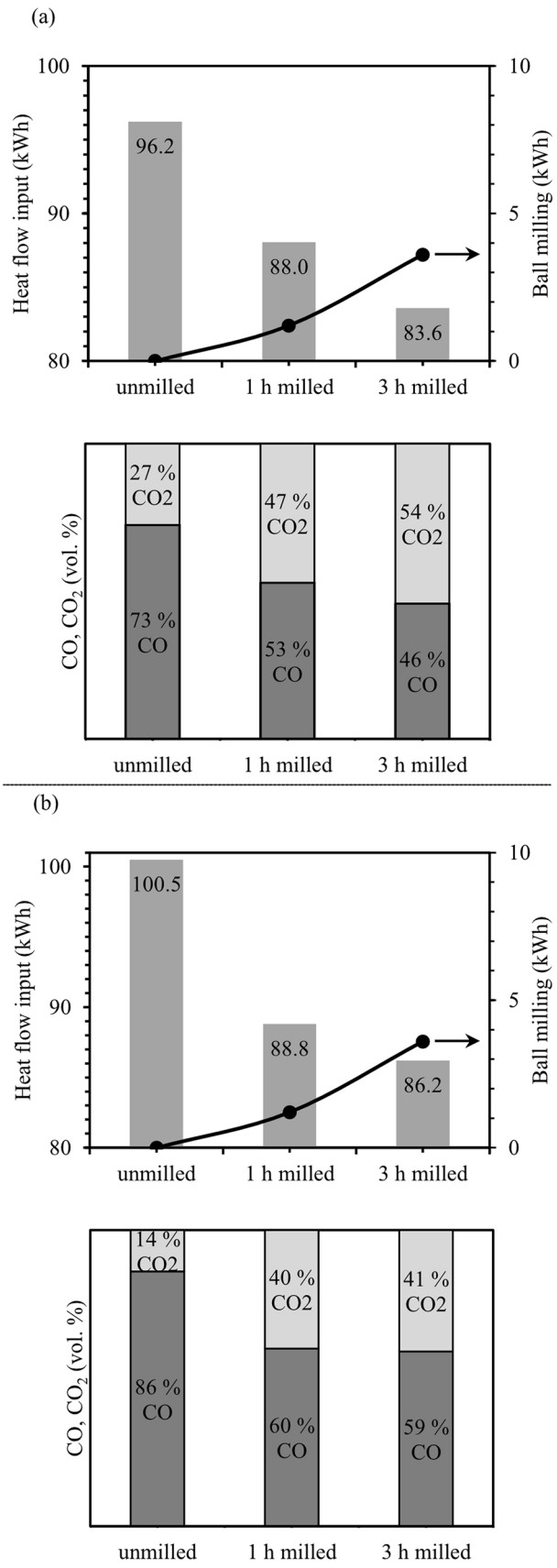

Fig. 10 Energy consumption and CO/CO_2 production during the reduction of **a** MixFeLCO and **b** MixFeNMC at 1450 °C, calculated by HSC chemistry

temperature range, which requires lower energy input. In addition, both the experimental and modeling results show that by increasing the milling time the CO/CO_2 ratio decreases and the final excess C increases.

Mass and energy balance simulations were also used to estimate the effect of milling on the CO_2 emissions of the process. The results of this estimation for MixFeLCO and MixFeNMC systems are presented in Fig. 11, in which the emissions are shown separately for direct emissions from the process (i.e., Scope I) and for indirect emissions from the energy production (i.e., Scope II). For Scope II emissions, specific CO_2 emissions of 0.820 kg/kWh, 0.030 kg/kWh and 0.012 kg/kWh were used for energy produced from fossil, renewable and nuclear sources, respectively [34]. The percentage values shown in the Fig. 13 indicate the reduction of CO_2 emissions due to milling in different cases.

The calculated exergy balances are depicted in Fig. 12. During the reduction of unmilled MixFeLCO, exergy emission is 2.27×10^5 kJ, which decreases to 2.09×10^5 and 2.04×10^5 kJ after 1 and 3 h of milling, respectively. This change in the reduction of MixFeNMC is from 2.40×10^5 kJ in the unmilled mixture to 2.15×10^5 and 2.14×10^5 kJ after 1 and 3 h of milling, respectively.

Copper System

As observed in the previous sections, milling for 3 h, compared to 1 h, does not significantly change the mass loss rate of the BM and Fe_2O_3-BM mixture. Therefore, the condition of 3 h of milling is omitted for the CuO-BM mixtures.

Figure 13 depicts the mass loss of the CuO-BM mixture during heating until 1450 °C. It can be seen that mass loss occurs with a higher rate after milling for 1 h. The effect of mechanical activation is mainly observable in the temperature range of 300–900 °C. For instance, at 700 °C, the mass loss increases by 4% and 11% after 1 h of milling in the LCO-CuO and NMC-CuO mixtures, respectively.

The XRD patterns of the reduced mixtures are presented in Fig. 14. Similar to what was observed in the iron system, in addition to graphite peaks, they are peaks of metallic phases, including Cu, Co, and Ni (particularly in MixCuNMC). The peak intensities in the iron and copper system are not comparable, because of different components, different grindability of materials and the fluorescence effect (even by using monochromator for suppressing the fluorescence) [33].

The chemical composition of the Cu-containing mixtures after reduction is listed in Table 4. The results of the unmilled and milled samples show that mechanical

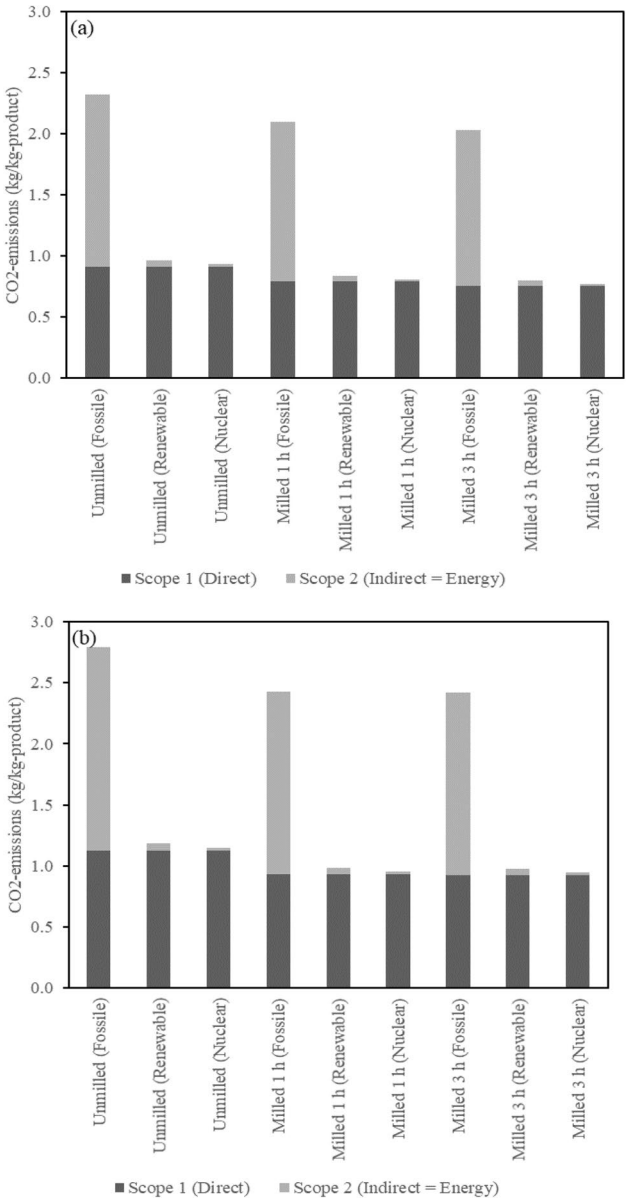

Fig. 11 Specific CO_2 emissions during reduction of **a** MixFeLCO, and **b** MixFeNMC at 1450 °C, calculated by HSC chemistry

activation significantly increases the final C that remains in the sample after reduction.

By comparing the TGA graphs in Fig. 13, it is seen that the mechanical activation affects the system from ~200–300 °C (beginning of CuO reduction) to ~1000 °C (MixCuLCO) and ~800 °C (MixCuNMC), where Cu begins to melt according to FactSage calculations. There

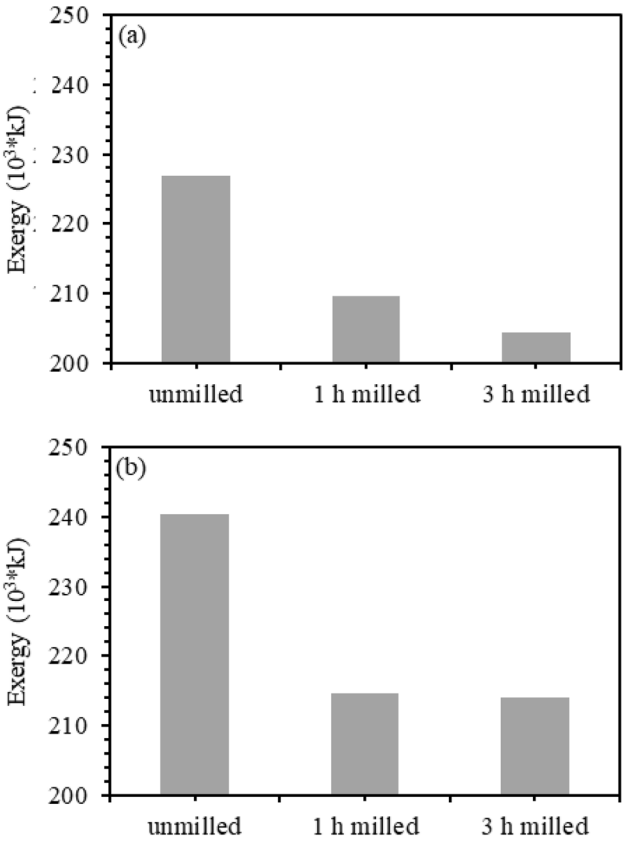

Fig. 12 Calculated exergy balance of **a** MixFeLCO, and **b** MixFeNMC reduction at 1450 °C

is almost no change after mechanical activation at higher temperatures. Generally, mechanical activation changes the surface properties of solid particles. When the system's main component melts, there is no other solid surface, and thus mechanical activation no longer affects the reaction kinetics.

Figure 15 demonstrates the results from mass and energy balance calculations. Similar to what was discussed in Iron system, milling of the CuO-BM mixture leads to higher reaction rates, which shifts the reduction occur to a lower temperature range; thus, less energy input is required. This also results in a lower CO/CO_2 ratio that increases the final amount of excess C after reduction.

According to what has been discussed for the MeO-BM mixtures, it can be stated that by applying mechanical activation and increasing the reduction rate, the efficiency of the reduction process can be increased. The C in the BM can be used to reduce more MeO, and then a lower temperature is required for the reduction.

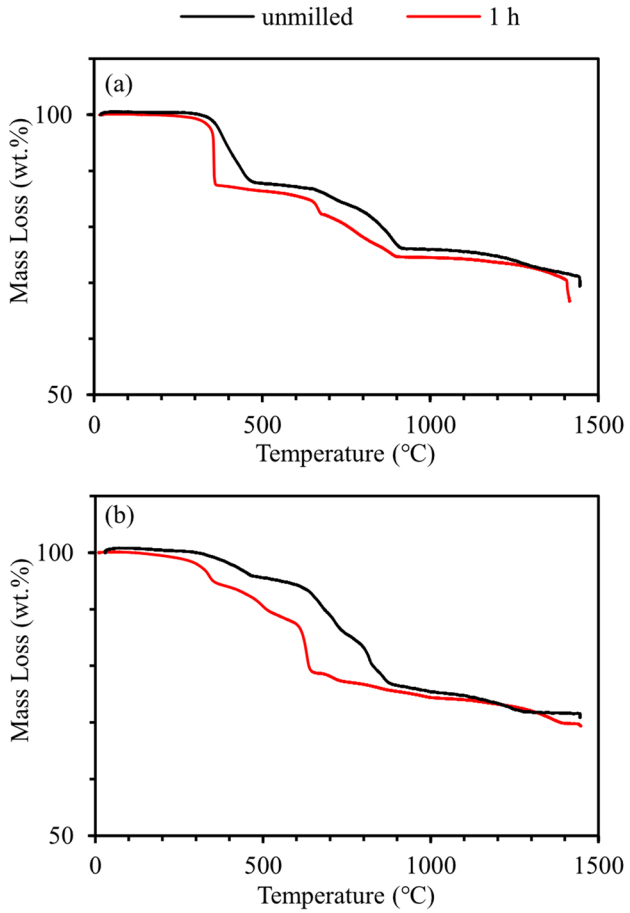

Fig. 13 Mass loss as a function of temperature during reduction of **a** MixCuLCO and **b** MixCuNMC before and after milling for 1 h

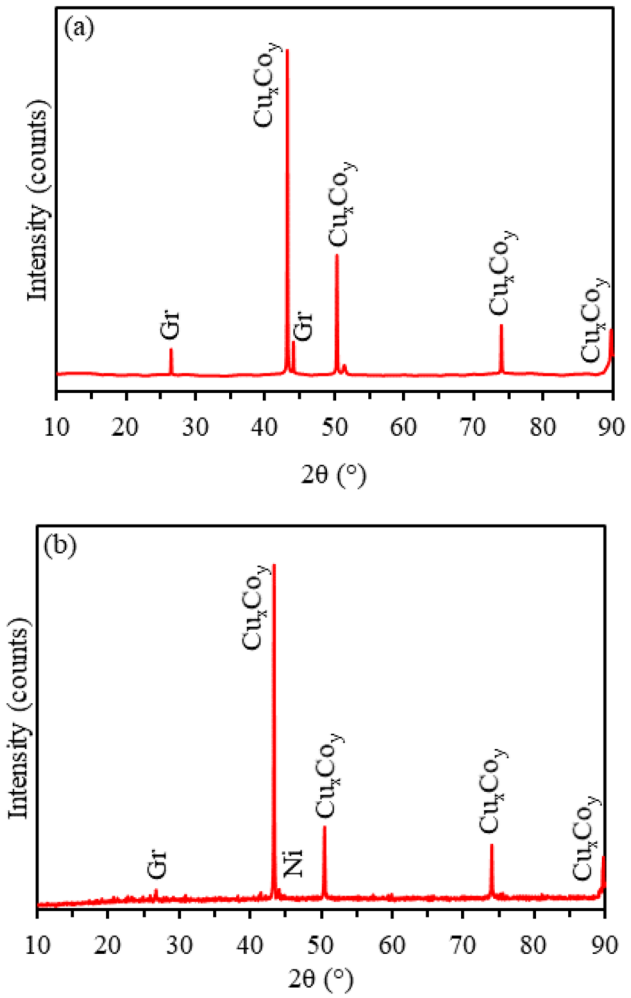

Fig. 14 XRD patterns of reduced **a** MixCuLCO and **b** MixCuNMC milled for 1 h

Mass and energy balance simulations were also used to estimate the effect of milling on the CO_2 emissions of the process. The results of this estimation for MixCuLCO and MixCuNMC systems are presented in Fig. 16, in which the emissions are shown separately for direct emissions from the process (i.e. Scope I) and for indirect emissions from the energy production (i.e. Scope II). For Scope II emissions, specific CO_2 emissions of 0.820 kg/kWh, 0.030 kg/kWh and 0.012 kg/kWh were used for energy produced from fossil, renewable and nuclear sources, respectively [34]. The percentage values shown in the Fig. 16 indicate the reduction of CO_2 emissions due to milling in different cases.

Exergy balance has been calculated in the Cu mixtures. As shown in Fig. 17, the exergy emission is 1.23×10^5 kJ for the reduction of unmilled MixCuLCO, which decreases to 0.67×10^5 kJ after an hour of milling. In the

Table 4 Chemical composition of unmilled and milled CuO-BM mixtures after reduction at 1450 °C

Mixture	Milling time	Chemical composition						
		Cu	Co	Mn	Ni	C	Li	Other
MixCuLCO	Unmilled	70.5 ± 0.2	25.0 ± 0.0	0.1 ± 0.0	0.1 ± 0.0	0.9 ± 0.1	1.4 ± 0.4	2.0
	1 h	70.5 ± 0.1	17.0 ± 0.1	0.0	0.0	8.9 ± 0.0	1.9 ± 0.6	1.8
MixCuNMC	Unmilled	84.9 ± 0.8	4.4 ± 0.0	3.2 ± 0.0	3.5 ± 0.0	2.0 ± 0.7	1.3 ± 0.4	0.7
	1 h	76.4 ± 0.3	3.7 ± 0.0	3.2 ± 0.0	3.4 ± 0.0	10.5 ± 0.3	1.6 ± 0.5	0.9

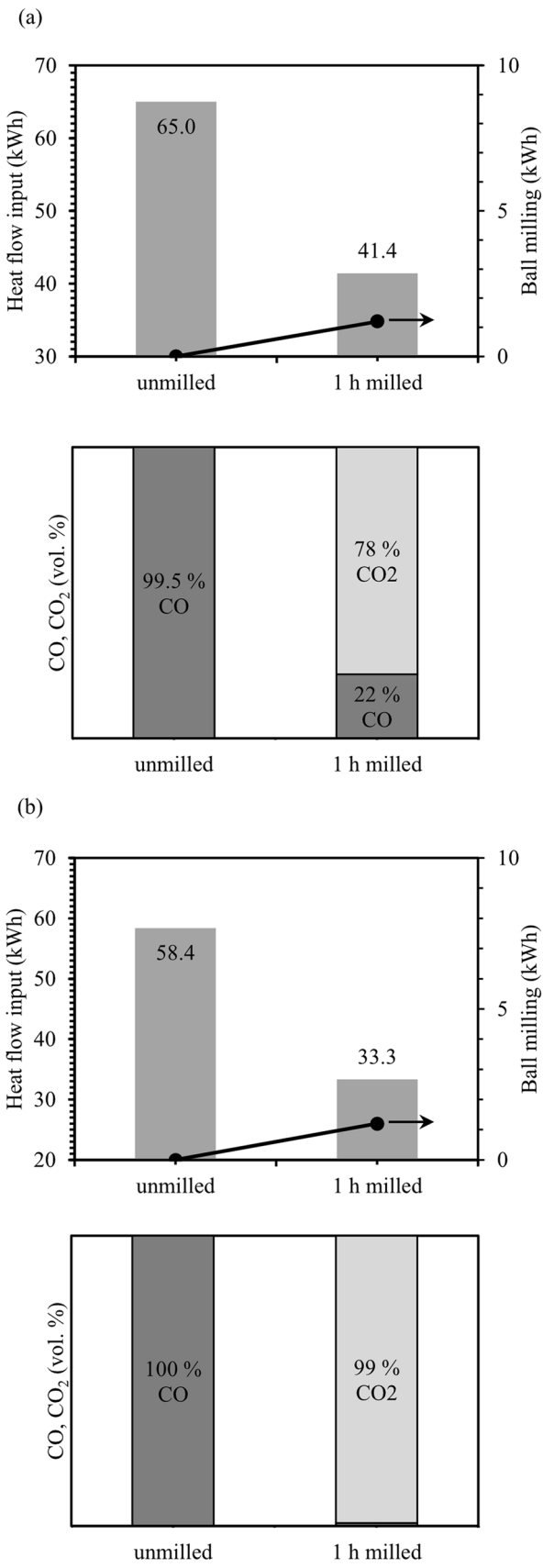

Fig. 15 Energy consumption and CO/CO_2 production during the reduction of **a** MixCuLCO and **b** MixCuNMC at 1450 °C, calculated by HSC chemistry

MixCuNMC, an hour of milling changes the exergy loss from 1.06×10^5 to 0.46×10^5 kJ.

Comparing to the iron system (Fig. 10), it has been seen in the copper system that mechanical activation has a more significant effect on lowering the required input energy. To explain, thermodynamics and kinetics of the reactions should be both taken into account. From the thermodynamic point of view, the reduction of CuO to metallic Cu is feasible at room temperature, while reduction of Fe_2O_3 requires elevated temperatures. Hence, the only factor that postpones the reduction of CuO to higher temperatures is kinetics of the reaction. Because of that, changing the kinetic parameters (decreasing the particle size) has a more significant effect on the copper system comparing to the iron system. By increasing the reduction rate, reduction shifts to a lower temperature range, which increases the CO_2/CO ratio. This results in consumption of a lower amount of C that equals to consumption of lower chemical energy, and consequently saving more energy.

Conclusions

In this research, it was attempted to address some of the major downsides of pyrometallurgical methods in recovering metallic elements from LIB BM: graphite loss, high energy consumption, and CO_2 emission. To avoid graphite loss, the feasibility of alloy making using BM was investigated by the addition of Fe_2O_3 and CuO to two types of BM (LCO and NMC). Regarding high energy consumption and CO_2 emission, mechanical activation was proposed as a solution. The experimental work showed that by adding MeO to BM (with a total C/O ratio of one), the added MeO was completely reduced to the metallic form, where Co (and Ni in NMC BM) would also be reduced. It was observed that mechanical activation increases the reduction rate; accordingly, the reduction reactions shift to a lower temperature range, and consequently, less energy is required for the reduction of BM and MeO-BM mixture. Another consequence of mechanical activation is that by lowering the temperature

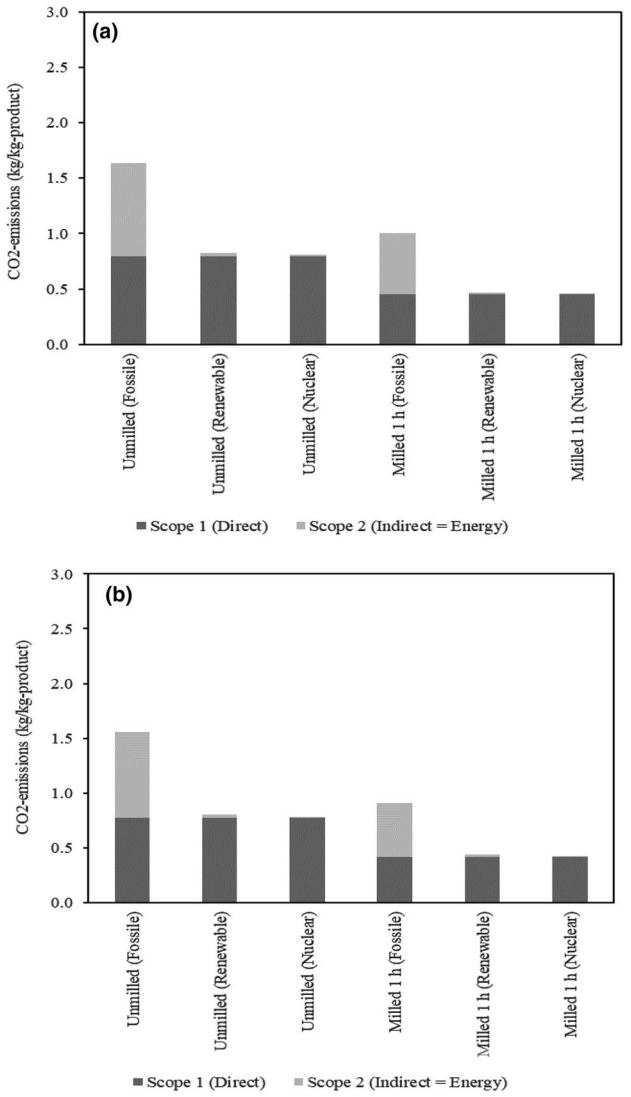

Fig. 16 Specific CO_2 emissions during reduction of **a** MixCuLCO, and **b** MixCuNMC at 1450 °C, calculated by HSC chemistry

range that reduction takes place, the ratio of CO_2/CO (as reduction products) increases, which leads to consumption of lower amount of C and lower total CO_2 emission. This effect increases the C remaining in the system. In general, mechanical activation enables the reduction of more MeO by the BM and decreases the energy consumption and CO_2 emission.

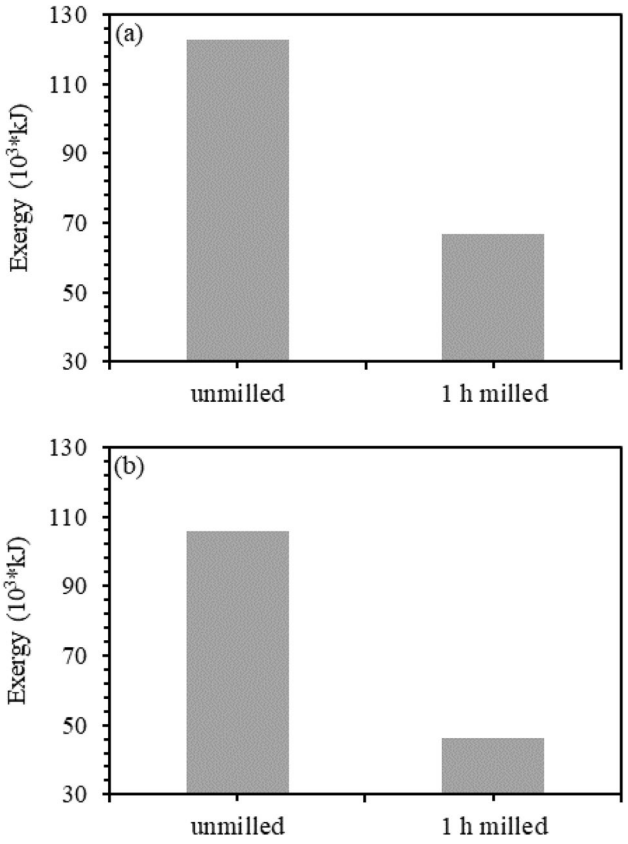

Fig. 17 Calculated exergy balance of **a** MixCuLCO, and **b** MixCuNMC reduction at 1450 °C

Funding Open access funding provided by Lulea University of Technology.

Declarations

Conflict of interest On behalf of all authors, the corresponding author states that there is no conflict of interest.

References

1. Kawamura H, LaFleur M, Iversen K, Cheng HWJ (2021) Lithium-ion batteries: a pillar for a fossil fuel-free economy. United Nations, Frontier Technology Issues, pp 1–10. https://www.un.org/development/desa/dpad/wp-content/uploads/sites/45/publication/FTI_July2021.pdf
2. Fan E, Li L, Wang Z, Lin J, Huang Y, Yao Y, Chen R, Wu F (2020) Sustainable recycling technology for li-ion batteries and beyond: challenges and future prospects. Chem Rev 120(14):7020–7063. https://doi.org/10.1021/acs.chemrev.9b00535
3. IEA (2020) Innovation in batteries and electricity storage. https://www.iea.org/reports/innovation-in-batteries-and-electricity-storage
4. The European Parliament and of the Council (2006) Directive 2006/66/EC of the European Parliament and of the Council of 6 September 2006 on batteries and accumulators and waste batteries and accumulators and repealing Directive 91/157/EEC. Official Journal of the European Union.
5. European Comission (2020) Critical raw materials resilience: charting a path towards greater security and sustainability. https://eur-lex.europa.eu/legal-content/EN/TXT/?uri=CELEX:52020DC0474
6. Pinegar H, Smith YR (2019) Recycling of end-of-life lithium ion batteries, Part I: commercial processes. J Sustain Metall 5(3):402–416. https://doi.org/10.1007/s40831-019-00235-9
7. Makuza B, Tian Q, Guo X, Chattopadhyay K, Yu D (2021) Pyrometallurgical options for recycling spent lithium-ion batteries: a comprehensive review. J Power Sources 491:229622. https://doi.org/10.1016/j.jpowsour.2021.229622
8. Pinegar H, Smith YR (2020) Recycling of end-of-life lithium-ion batteries, Part II: laboratory-scale research developments in mechanical, thermal, and leaching treatments. J Sustain Metall 6(1):142–160. https://doi.org/10.1007/s40831-020-00265-8
9. Meshram P, Pandey BD, Mankhand TR (2014) Hydrometallurgy Extraction of lithium from primary and secondary sources by pre-treatment, leaching and separation: a comprehensive review. Hydrometallurgy 150:192–208. https://doi.org/10.1016/j.hydromet.2014.10.012
10. Or T, Gourley SWD, Kaliyappan K, Yu A, Chen Z (2020) Recycling of mixed cathode lithium-ion batteries for electric vehicles: current status and future outlook. Carbon Energy 2(1):6–43. https://doi.org/10.1002/cey2.29
11. Velázquez-Martínez O, Valio J, Santasalo-Aarnio A, Reuter M, Serna-Guerrero R (2019) A critical review of lithium-ion battery recycling processes from a circular economy perspective. Batteries 5(4):68. https://doi.org/10.3390/batteries5040068
12. Mossali E, Picone N, Gentilini L, Rodrìguez O, Pérez JM, Colledani M (2020) Lithium-ion batteries towards circular economy: a literature review of opportunities and issues of recycling treatments. J Environ Manage 264:110500. https://doi.org/10.1016/j.jenvman.2020.110500
13. Zheng X, Zhu Z, Lin X, Zhang Y, He Y, Cao H, Sun Z (2018) A mini-review on metal recycling from spent lithium ion batteries. Engineering 4(3):361–370. https://doi.org/10.1016/j.eng.2018.05.018
14. Hanisch C, Loellhoeffel T, Diekmann J, Markley KJ, Haselrieder W, Kwade A (2015) Recycling of lithium-ion batteries: a novel method to separate coating and foil of electrodes. J Clean Prod 108:301–311. https://doi.org/10.1016/j.jclepro.2015.08.026
15. Hu X, Mousa E, Ye G (2021) Recovery of Co, Ni, Mn, and Li from Li-ion batteries by smelting reduction—Part II: a pilot-scale demonstration. J Power Sources 483:229089. https://doi.org/10.1016/j.jpowsour.2020.229089
16. Lombardo G, Ebin B, Foreman MR, Steenari BM, Petranikova M (2020) Incineration of EV Lithium-ion batteries as a pretreatment for recycling—determination of the potential formation of hazardous by-products and effects on metal compounds. J Hazard Mater 393(January):122372. https://doi.org/10.1016/j.jhazmat.2020.122372
17. Diaz F, Wang Y, Moorthy T, Friedrich B (2018) Degradation mechanism of nickel-cobalt-aluminum (NCA) cathode material from spent lithium-ion batteries in microwave-assisted pyrolysis. Metals 8(8):565. https://doi.org/10.3390/met8080565
18. Kwon OS, Sohn I (2020) Fundamental thermokinetic study of a sustainable lithium-ion battery pyrometallurgical recycling process. Resour Conserv Recycl 158:104809. https://doi.org/10.1016/j.resconrec.2020.104809
19. Lombardo G, Ebin B, St Foreman MRJ, Steenari BM, Petranikova M (2019) Chemical transformations in Li-ion battery electrode materials by carbothermic reduction. ACS Sustain Chem Eng 7(16):13668–13679. https://doi.org/10.1021/acssuschemeng.8b06540
20. Sommerfeld M, Vonderstein C, Dertmann C, Klimko J, Oráč D, Miškufová A, Havlík T, Friedrich B (2020) A combined pyro-and hydrometallurgical approach to recycle pyrolyzed lithium-ion battery black mass part 1: Production of lithium concentrates in an electric arc furnace. Metals 10(8):1–27. https://doi.org/10.3390/met10081069
21. Hu H, Chen Q, Yin Z, Zhang P (2003) Thermal behaviours of mechanically activated pyrites by thermogravimetry (TG). Thermochim Acta 398(1–2):233–240. https://doi.org/10.1016/S0040-6031(02)00390-8
22. Hu H, Chen Q, Yin Z, Zhang P, Ye L (2003) The thermal behaviour of mechanically activated galena by thermogravimetry analysis. Metall Mater Trans A 34(13):793–797. https://doi.org/10.1007/s11661-003-1007-y
23. Hu H, Chen Q, Yin Z, Zhang P, Zou J, Che H (2002) Study on the kinetics of thermal decomposition of mechanically activated pyrites. Thermochim Acta 389(1–2):79–83. https://doi.org/10.1016/S0040-6031(01)00850-4
24. Kosmac T, Courtney TH (1992) Milling and mechanical alloying of inorganic nonmetallics. J Mater Res 7(6):1519–1525. https://doi.org/10.1557/JMR.1992.1519
25. Pourghahramani P, Forssberg E (2007) Reduction kinetics of mechanically activated hematite concentrate with hydrogen gas using nonisothermal methods. Thermochim Acta 454(2):69–77. https://doi.org/10.1016/j.tca.2006.12.023
26. Zdujić M, Jovalekić Č, Karanović L, Mitrić M, Poleti D, Skala D (1998) Mechanochemical treatment of α-Fe2O3 powder in air atmosphere. Mater Sci Eng, A 245(1):109–117. https://doi.org/10.1016/s0921-5093(97)00715-6
27. Welham NJ (2002) Activation of the carbothermic reduction of manganese ore. Int J Miner Process 67(1–4):187–198. https://doi.org/10.1016/S0301-7516(02)00045-5
28. Babanejad S, Ahmed H, Andersson C, Samuelsson C, Lennartsson A, Hall B, Arnerlöf L (2022) High-temperature behaviour of spent Li-ion battery black mass in inert atmosphere. J Sustain Metall 8(1):566–581. https://doi.org/10.1007/s40831-022-00514-y
29. Bale CW, Bélisle E, Chartrand P, Decterov SA, Eriksson G, Gheribi AE, Hack K, Jung IH, Kang YB, Melançon J, Pelton AD, Petersen S, Robelin C, Sangster J, Spencer P, Ende M.-A. Van (2016) FactSage thermochemical software and databases—2010–2016. Calphad 54:35–53
30. Jung SM, Yi SH (2013) A kinetic study on carbothermic reduction of hematite with graphite employing thermogravimetry and quadruple mass spectrometry. Steel Res Int 84(9):908–916. https://doi.org/10.1002/srin.201200310

31. Szendrei T, Van Berge PC (1981) Thermogravimetry and evolved gas analysis of the reduction of hematite (Fe2O3) with graphite. Thermochim Acta 44(1):11–19. https://doi.org/10.1016/0040-6031(81)80266-3
32. Kirakosyan H, Minasyan T, Niazyan O, Aydinyan S, Kharatyan S (2016) DTA/TG study of CuO and MoO3 co-reduction by combined Mg/C reducers. J Therm Anal Calorim 123(1):35–41. https://doi.org/10.1007/s10973-015-4919-z
33. Mos YM, Vermeulen AC, Buisman CJN, Weijma J (2018) X-Ray diffraction of iron containing samples: the importance of a suitable configuration. Geomicrobiol J 35(6):511–517. https://doi.org/10.1080/01490451.2017.1401183
34. World Nuclear Association (2021) Carbon dioxide emissions from electricity. https://www.world-nuclear.org/information-library/energy-and-the-environment/carbon-dioxide-emissions-from-electricity.aspx